Published in final edited form as:
Magn Reson Med. 2013 July ; 70(1): 147–154. doi:10.1002/mrm.24429.

One Component? Two Components? Three? The Effect of Including a Non-Exchanging 'Free" Water Component in Multicomponent Driven Equilibrium Single Pulse Observation of T1 & T2 (mcDESPOT)

Sean C.L. Deoni[1], **Lucy Matthews**[3,4], and **Shannon H. Kolind**[2,3]

[1]Advanced Baby Imaging Lab, School of Engineering, Brown University, Providence, RI, USA

[2]Department of Neuroimaging, King's College London, Institute of Psychiatry, London, UK

[3]Oxford Centre for Functional Magnetic Resonance Imaging of the Brain (FMRIB), University of Oxford. UK

[4]Department of Clinical Neurology, Oxford University and Oxford Radcliffe Hospitals NHS Trust, UK

Abstract

Quantitative myelin content imaging provides novel and pertinent information related to underlying pathogenetic mechanisms of myelin-related disease, or disorders arising from aberrant connectivity. Multicomponent Driven Equilibrium Single Pulse Observation of T_1 and T_2 (mcDESPOT) is a time-efficient multicomponent relaxation analysis technique that provides estimates of the myelin water fraction (MWF), a surrogate measure of myelin volume. Unfortunately, mcDESPOT relies on a two water-pool model (myelin-associated water, and intra/extra cellular water), which is inadequate within partial-volume voxels, i.e. containing brain tissue and ventricle or meninges, resulting in MWF under-estimation. To address this, a third, non-exchanging 'free-water' component was introduced to the mcDESPOT model. Numerical simulations and experimental in vivo data show the model to perform advantageously within partial volume regions whilst providing robust and reproducible results. It is concluded that this model is preferable for future studies and analysis.

Keywords

White Matter Imaging; Human Brain Imaging; Myelin Imaging; Myelin Water Fraction; Quantitative Imaging

Introduction

Non-invasive assessment of myelin content provides salient information in de and dys-myelinating disorders as well as in neurological and psychiatric disorders suspected of arising from altered brain connectivity. Multi-component analysis of relaxation data (MCR) provides a surrogate measure of myelin volume through a quantitative metric, termed the myelin water fraction, and defined as the proportion of water trapped within the lipid bilayers of the myelin sheath relative to the total water contained within the imaging voxel

Address Correspondence to: Sean Deoni, Advanced Baby Imaging Lab, School of Engineering, Brown University, Providence, RI, USA, 02912, Tel. # +1 401.683.6468, sdeoni@mac.com.

(1). Prior work examining myelin water fraction estimates derived from T_2 decay data of normal and pathological tissue have demonstrated strong correlations with histological myelin content assessments (2,3), demonstrating its utility in investigations of white matter pathology (4-6). Unfortunately, conventional multiple-echo T_2 techniques are time consuming and requiring lengthy scan times (i.e. 16 minutes for approx. 8-12 contiguous slices) (7).

mcDESPOT (multi-component Driven Equilibrium Single Pulse Observation of T_1 and T_2) (8), is an alternative MCR approach that affords improved time efficiency and the ability to acquire whole-brain data in clinically feasible scan times. Whilst T_2-based approaches derive the myelin water fraction from a series spin-echo measurements acquired over an echo time range, mcDESPOT utilizes a series of spoiled gradient echo (SPGR, spoiled FLASH) and fully-balanced steady-state free precession (bSSFP) data acquired over a range of flip angles. Additional acquisitions may be included to correct for main (B_0) and transmit (B_1) magnetic field inhomogeneities (9). To calculate the myelin water fraction, SPGR and bSSFP signal models incorporating two exchanging water pools (water trapped within the myelin sheath; and a combined pool comprised of water inside and outside the myelinated axons, together termed the intra/extra-cellular, IE, water) are fit to the data.

Though some groups have sought to resolve the signal from water within the axon (axonal water), from that outside the axon (extra-axonal water) through additional data acquisition or inclusion of T_1 information (10, 11), conventional T_2 analysis reliably provides two independent pools within white matter (1).

Voxels containing heterogeneous tissues, for example containing portions of brain tissue and ventricle or meninges, or within necrotic ‘black holes’ and tumors, may not be suitable modeled using a straight-forward two-component model. In these areas, the very slow relaxing ‘free’ water (i.e., the cerebral spinal fluid within the ventricles) is not adequately accounted for by mcDESPOT, potentially causing under-estimation of the myelin water fraction and/or over-estimation of each pool’s T_1 and T_2 values. In these regions it is logical to include a third, non-exchanging, water pool into the mcDESPOT model.

In this paper, we describe the inclusion of a third non-exchanging and slowly-relaxing water pool into the SPGR and bSSFP signal models. Through numerical simulations, we investigate the accuracy and precision of this three-pool model compared to the prior two-pool approach. The simulation results are confirmed in vivo using experimental results from a broad range of participants, and the method’s reproducibility is evaluated using repeated scans of the same individual. Results show the three-pool model provides more robust myelin water fraction estimation in partial volume areas, particularly in regions bordering brain tissue and the ventricles and meninges with high reproducibility.

Theory

3 Pool Model

As presented previously (12-14), the two-component steady-state SPGR and bSSFP magnetizations (M^{SS}_{SPGR} and M^{SS}_{bSSFP}) are written in matrix notation as

$$M^{SS}_{SPGR}=(I - e^{A_{SPGR}\times TR}\cos\alpha)^{-1} \times M_{SPGR}(I - e^{A_{SPGR}\times TR})\sin\alpha \quad [1]$$

and

$$M_{bSSFP}^{SS}=\left[I-e^{A_{bSSFP}\times TR}R(\alpha)\right]^{-1}\times(e^{A_{bSSFP}\times TR}-I)A_{bSSFP}^{-1}C, \quad [2]$$

where I is the identity matrix, and M_{SPGR}, M_{bSSFP}, A_{SPGR}, A_{bSSFP}, C and $R(\alpha)$ are matrices containing the relative water pool volume fraction, relaxation, off-resonance, exchange rate, and excitation flip angle terms defined in Appendix A. M_{SPGR}^{SS} and M_{bSSFP}^{SS} are column vectors containing the x, y and z components of the steady-state magnetization,

$$M_{SPGR}^{SS}=\left[M_{z,M}^{SPGR,SS},M_{z,IE}^{SPGR,SS}\right]^{T} \quad [3]$$

and

$$M_{bSSFP}^{SS}=\left[M_{x,M}^{bSSFP,SS},M_{x,IE}^{bSSFP,SS},M_{y,M}^{bSSFP,SS},M_{y,IE}^{bSSFP,SS},M_{z,M}^{bSSFP,SS},M_{z,IE}^{bSSFP,SS}\right]^{T}. \quad [4]$$

The M and IE subscripts denote the myelin-associated and intra/extra-cellular water pools, respectively. T denotes the transpose of the matrix. In the case of SPGR, only the longitudinal magnetization is considered, with the transverse magnetization ideally spoiled prior to each radio-frequency (RF) excitation pulse.

The measured two-component SPGR and bSSFP signals, therefore, are

$$S_{SPGR}^{2-Component}=M_{z,M}^{SPGR,SS}+M_{z,IE}^{SPGR,SS} \quad [5]$$

and

$$S_{bSSFP}^{2-Component}=M_{x,M}^{bSSFP,SS}+M_{x,IE}^{bSSFP,SS}+i\left(M_{y,M}^{bSSFP,SS}+M_{y,IE}^{bSSFP,SS}\right). \quad [6]$$

To incorporate a third non-exchanging water pool into these models, we expand the M_{SPGR}, M_{bSSFP}, A_{SPGR}, A_{bSSFP}, C and $R(\alpha)$ matrices as shown in Appendix B. M_{SPGR}^{SS} and M_{bSSFP}^{SS} are re-defined as

$$M_{SPGR}^{SS}=\left[M_{z,M}^{SPGR,SS},M_{z,IE}^{SPGR,SS},M_{z,F}^{SPGR,SS}\right]^{T} \quad [7]$$

and

$$M_{bSSFP}^{SS}=\left[M_{x,M}^{bSSFP,SS},M_{x,IE}^{bSSFP,SS},M_{x,F}^{bSSFP,SS},M_{y,M}^{bSSFP,SS},M_{y,IE}^{bSSFP,SS},M_{y,F}^{bSSFP,SS},M_{z,M}^{bSSFP,SS},M_{z,IE}^{bSSFP,SS},M_{z,F}^{bSSFP,SS}\right]^{T}, \quad [8]$$

where the F subscript denotes the third non-exchanging ‘free’ water pool.

The three-component SPGR and bSSFP signal, therefore, is given by

$$S_{SPGR}^{3-Component}=M_{z,M}^{SPGR,SS}+M_{z,IE}^{SPGR,SS}+M_{z,F}^{SPGR,SS} \quad [9]$$

and

$$S_{bSSFP}^{3-Component}=M_{x,M}^{bSSFP,SS}+M_{x,IE}^{bSSFP,SS}+M_{x,F}^{bSSFP,SS}+i\left(M_{y,M}^{bSSFP,SS}+M_{y,IE}^{bSSFP,SS}+M_{y,F}^{bSSFP,SS}\right). \quad [10]$$

In this model we have assumed the slow-relaxing 'free' water pool to be non-exchanging with respect to the T_1 and T_2 times. This is likely a safe assumption for ventricular and meningeal water, which needs to cross the blood-brain barrier before mixing with the tissue water pools.

Discrete Fitting of the 3 Pool Model

To derive estimates of $T_{1,M}$, $T_{1,IE}$, $T_{1,F}$, $T_{2,M}$, $T_{2,IE}$, $T_{2,F}$, M_F, F_F, and τ_M, Eqns. [9] and [10] are fit to acquired multiple flip angle data using a stochastic region contraction (SRC) approach (9, 15). SCR comprises the following 6 steps: 1. Likely value ranges for each free-parameter are first defined; 2) N_S Potential solution sets are then generated by randomly selecting values for each free-parameter from the defined ranges; 3) The least-squares residual for each potential solution is calculated, and the solutions rank-ordered; 4) The top N_T solutions are identified, and the minimum and maximum value of each free parameter contained within this sub-set are determined; 5) The identified minimum and maximum values are used to re-define the possible value ranges (i.e., contracting the search-space); and 6) Return to step #2 and repeat until convergence is achieved or some termination criteria is met.

To fit our models, we define the following. Initial value ranges are: 250ms ≤ $T_{1,M}$ ≤ 750ms; 250ms ≤ $T_{1,IE}$ ≤ 3500ms; 1500ms ≤ $T_{1,F}$ ≤ 7500ms; 0ms ≤ $T_{2,M}$ ≤ 150ms; 0ms ≤ $T_{2,IE}$ ≤ 250ms; 150ms ≤ $T_{2,F}$ ≤ 1000ms; 0.00 ≤ M_F ≤ 0.49; 0.00 ≤ F_F ≤ 0.75; and 25ms ≤ τ_M ≤ 1500ms. Additional constraints, $IE_F = 1.00 - (M_F + F_F)$; and $M_F + F_F \leq 0.95$, are imposed. These value ranges were chosen followed consideration of prior literature values (1, 10, 11).

N_S = 5000 sets of $<T_{1,M}, T_{1,IE}, T_{1,F}, T_{2,M}, T_{2,IE}, T_{2,F}, M_F, F_F, \tau_M>$ are generated by randomly choosing each parameter from a uniform distribution.

Sum-of-squares residuals are calculated following normalization of the theoretical and acquired data. The SPGR and bSSFP data are independently normalized with respect to their mean values.

From the 5000 $<T_{1,M}, T_{1,IE}, T_{1,F}, T_{2,M}, T_{2,IE}, T_{2,F}, M_F, F_F, \tau_M>$ potential solutions, the top $N_T = 50$ sets are used to contract each parameter's value range.

The algorithm is repeated until the difference between the minimum and maximum values of each parameter drops below 1%, or until a total number of repeats ($N_R = 6$) is performed.

Methods

Simulation Methods

Numerical simulations were used to investigate the accuracy and precision in fitting the three-pool model over a range of experimental conditions. We also compared the results of the three-pool model to results derived using the two-pool mode.

Theoretical data were calculated using Eqns. [9] and [10] for F_F ={0, 0.10, 0.20, 0.30, 0.40 and 0.50}; for M_F = {0.05, 0.1, 0.15, 0.2 and 0.25}. This provided a 6×5 F_F vs. M_F grid. $T_{1,M}$, $T_{1,IE}$, $T_{1,F}$, $T_{2,M}$, $T_{2,IE}$, $T_{2,F}$, and τ_M were held constant at 465ms, 965ms, 3500ms, 12ms, 90ms, 250ms, and 125ms, respectively (1, 10, 11).

For each simulation, 50,000 realizations were calculated from theoretical data with Gaussian-distributed additive noise. The two and three-pool models were fit to the simulated data, with the accuracy (absolute percent difference between the known and estimated

values) and precision (mean divided by the standard deviation) of the M_F estimates evaluated and compared.

In Vivo Data Acquisition

To evaluate *in vivo* performance, CNS data were acquired across a broad range of participants representing a mix of healthy and pathological conditions. Data were acquired of healthy 3 month old male infant; a healthy 24 year-old adult male; and an 81 male AD patient (mini-mental state exam score = 18). Cervical spine data were acquired of a 30 year-old female MS patient. To provide insight into the method's reproducibility, data were acquired of the 24 year-old adult male on 5 separate occasions spanning 5 weeks. To inform on inter-subject variability, data were acquired of 10 1-year old infants (353-383 days of age, 7 female).

All scanning was performed following informed consent and with IRB approval from the host institution. Data were acquired on a Siemens Tim Trio scanner with a 12-channel head and neck RF array or spine array and the following acquisition parameters.

Infant Brain Acquisition Strategy—Whole-brain sagittal orientation with a $16cm^2$ × 15cm field of view (FOV) and 96 × 96 × 88 acquisition matrix. *SPGR*: TE/TR = 5.5 ms / 13 ms; flip angles = (2, 3, 4, 5, 6, 7, 10 and 14)°; receiver bandwidth (BW) = 350 Hz/voxel *bSSFP:* TE/TR = 5.3 ms / 10.5 ms; flip angles = (11, 16, 19, 23, 27, 35, 50 and 70)°; BW = 350 Hz/voxel. Reduced resolution (half-size in each phase-encode direction) inversion-prepared (IR-) SPGR images were also acquired matched with the SPGR parameters and inversion delays of 50ms and 850ms to help correct for flip angle errors (9). The bSSFP data were acquired with two RF phase-cycling patterns (0 and 180°) to correct for B_0 inhomogeneity (9).

Adult Brain Acquisition Strategy—Whole-brain sagittal orientation with a $22cm^2$ × 17cm FOV and 128 × 128 × 98 acquisition matrix. *SPGR*: TE/TR = 2.4 ms / 5.4 ms; flip angles = (3, 4, 5, 6, 7, 9, 13 and 18)°; BW = 380 Hz/voxel *bSSFP:* TE/TR = 2.2 ms / 4.4 ms; flip angles = (10, 13, 17, 20, 23, 30, 43, and 60)°; BW = 560 Hz/voxel. A reduced resolution inversion-prepared (IR-) SPGR image was also acquired with an inversion delay of 450ms, and the bSSFP data were acquired with 0 and 180 degree RF phase-cycling patterns.

Adult Spine Acquisition Strategy—Whole cervical-spine sagittal orientation with a $20cm^2$ × 15cm FOV and 112 × 224 × 128 acquisition matrix. *SPGR*: TE/TR = 2.7 ms / 6.1 ms; 8 linearly spaced flip angles between 1 and 18°; BW = 400 Hz/voxel *bSSFP:* TE/TR = 2.3 ms / 4.6 ms; 8 linearly spaced flip angles between 5 and 45°; BW = 600 Hz/voxel. A reduced resolution inversion-prepared (IR-) SPGR image was also acquired with an inversion delay of 750ms, and the bSSFP data were acquired with 0 and 180 degree RF phase-cycling patterns.

Following acquisition, the individual flip angles images for each participant were linearly aligned to account for subtle intra-scan motion; non brain or spine signal was removed from each image, and the two and three-pool models fit voxel-wise to the data.

To compare the models, the two-pool M_F map was subtracted from the corresponding three-pool M_F map. It was expected that differences would be found bordering the ventricles and sulci, with no difference shown in the white and grey matter.

To examine the *in vivo* inter-scan reproducibility of the method, 5 sets of healthy adult repeat data were linearly aligned and voxel-wise measures of the coefficient of variation

(CoV) of the M_F maps were calculated. Likewise, inter-subject variability was evaluated by calculating voxel-wise CoV measures across 10 healthy 1 year old infants.

Results

Simulation Results

Figure 1 displays the myelin water fraction sub-component of the simulation results exploring the performance of the two and three-component models across the range of M_F and F_F values. As might have been expected, as the free-water compartment size (F_F) was increased, the two-pool M_F value became increasingly under-estimated. In a further attempt to accommodate the additional water pool, the IE water T_1 and myelin water residence time values were increasing over-estimated as F_F increased (not shown). In contrast, as hoped, the 3-pool model accommodates the increasing free water fraction well, with no M_F under-estimation or IE water T_1 over-estimation observed. Both models were found to provide comparable myelin water T_1 and T_2 values. Accuracy of the three-pool MWF values was also found to be high across the experimental conditions examined, with less than 10% error noted.

To shed light on the uniqueness of solution found, Figure 1 also contains histograms showing the distribution of the fitted myelin water and free water fraction parameters for the 50,000 simulation realizations for the case of $M_F = 0.1$ and $F_F = 0.20$. If the algorithm converged non-uniquely, we would expect to see multiple peaks within these parameter histograms, or in the worse case, a uniform distribution. The results show Gaussian distributions for each parameter, centered about the 'true' value, suggesting the algorithm is converging to the same solution repeatedly. Mean and standard deviation values are given for each parameter, with the 'true' value also given in red type. While not shown, the histogram results for the other fitted parameters were also Gaussian shaped with mean, standard deviation and **true** values of: $T_{1,M}$ = (460ms, 13ms, **465ms**), $T_{1,IE}$ = (979ms, 18ms, **965ms**), $T_{1,F}$ = (3527ms, 150ms, **3500ms**), $T_{2,M}$ = (11.6ms, 0.52ms, **12ms**), $T_{2,IE}$ = (90ms, 2.4ms, **90ms**), $T_{2,F}$ = (262ms, 26ms, **250ms**) and τ_M = (126ms, 28ms, **125ms**).

In Vivo Data Results

In vivo data results are shown in Figs. 2 and 3. Figure 2 contains a comparison of the 2 and 3-pool model derived M_F maps, alongside reference anatomical images and the 3-pool free water fraction (F_F) maps the healthy infant and healthy adult, as well as the MS and AD patient. Differences between the 2 and 3-pool M_F is most readily visualized in the difference (3-pool minus 2-pool result) map. For each participant, the difference between the two models is most apparent in partial volume voxels - those bordering the ventricles and meninges in the brain, and along the surface of the spinal cord. In these areas, the 2-pool model under-estimates the myelin volume fraction as predicted by the numerical simulations (Fig. 1). This effect is particularly evident in the AD patient data, where regions of the caudate nucleus and forceps major do not appear in the 2-pool M_F map. These areas are, however, visible in the 3-pool map.

Within more homogeneous white and grey matter, the two models provide comparable results. We calculated a M_F difference of less than 0.01 (3%) in white matter. This result is also consistent with the numerical simulations (Fig. 1). Model preference is quantified in the final panel of Fig. 2, which compares the two and three-pool model fit residuals for the AD patient, as well as results of a model selection approach using the bayesian information criterion (BIC, 16), which shows the 3-pool model to be justified over the majority of brain voxels. Further exploration of this is shown in Fig. 3, which shows raw data vs. flip angle curves for two different brain regions of interest (obtained from the older AD patient) and

reconstructed 2-pool and 3-pool model curves. Though subtle, differences are apparent between the 2 models. Calculated BIC metrics are shown on each curve, showing the 3-pool model to be preferred in both cases.

Figure 4 shows results of the single-subject (24 year old adult male scanned 5 times) repeatability (a) and multi-subject (10 1 year old infants) inter-subject reproducibilities (b) studies. Also shown in Fig. 4 is the result of an additional study of fitting algorithm stability. The stochastic nature of the fitting method is a potential source of error in mcDESPOT. To better understand this potential source of error, the fitting was repeated on the same data 500 times and the CoV of the estimates calculated. A slice through this CoV map is shown in Fig. 4c.

A slice through the inter-scan CoV map is shown in Fig. 4a, with average CoV measures obtained from 4 brain regions (frontal, occipital and cerebellar white matter, and thalamus) are noted in Table 1. The weighted average CoV across all four regions was 0.059.

Results of the algorithmic stability analysis are shown in Fig. 4c. The CoV, averaged over the whole slice was 0.0094, indicating the algorithm converges similarly despite it's random nature. This is an important result, showing not only stability of the algorithm, but also of the model itself. A potential issue encountered in fitting complex models is the occurrence of local minima: multiple parameter sets providing similar curves and model residuals. If this were true of the 3-pool model used herein, we would have expected to see low reproducibility in Fig. 4c, reflecting essentially random results from each solution iteration. The high reproducibility noted suggests the fitting algorithm consistently converges to the same unique solution, as was previously shown in the simulation results (Fig. 1) Improved reproducibility might be achieved through increasing the number of iterations of the algorithm, or increasing the number of samples taken at each iteration. Both, however, would increase computation time, currently ~14 hours (on an 8-core Intel I7 2.66GHz MacPro).

Discussion and Conclusions

Reliable estimation of myelin content has inherent interest in the study of de and dys-myelinating disorders, as well as neurodevelopmental or psychiatric disorders that may be associated with aberrant brain connectivity.

mcDESPOT is a potentially rapid and whole-brain quantitative MCR technique that may offer new opportunities for investigating the etiology and pathology of these disorders as well as normative development (17). However, to be of clinical or diagnostic utility, the method must provide robust results that adequately characterize the underlying tissue. Many disorders, including MS and AD, are associated with marked brain atrophy and gross anatomical lesions beyond focal or widespread myelin alteration. These pathological hallmarks may confound the interpretation of mcDESPOT results as the conventional two-pool mcDESPOT model approach may under-estimate the myelin water fraction in regions containing mixtures of brain tissue and free or bulk water, leading to the erroneous interpretation of advanced pathology, or in the 'staging' of the disease course.

In an effort to account for this, we have included an additional non-exchanging water pool to the model, and have evaluated this expanded approach through numerical simulations and *in vivo* imaging data.

Within homogeneous white and grey matter, results show the 3-pool models deviates negligibly (less than 3%) from the 2-pool model. This small difference may reflect reduced accuracy owing to the increased number of free parameters that must be fit in the expanded

model. Alternatively, this difference may be anatomically relevant, possibly (though unlikely) reflecting a vascular compartment. As the bulk water pool fraction increases, numerical simulations show an increasing under-estimation of the myelin water fraction. This is visualized *in vivo* within boundary voxels between grey matter or spinal cord and CSF spaces. The 3-pool model effectively recovers this under-estimation, as most easily observed within the AD patient data. Examination of the BIC map for this patient shows that in these areas the 3-pool model is justified by the data.

A potential limitation of the model proposed herein is that of no exchange between the 'tissue' water and the free bulk water. This assumption is likely justified within the ventricles and meninges, since water must cross the blood-brain barrier. However, no such barrier exists in the case of edema, corresponding to pathologies such as black holes or white matter hyperintensities. Omission of free water exchange may result in a systematic bias in the calculated free water fraction. This may explain the non-zero free water component found within the homogeneous white matter in the *in vivo* data. Inclusion of exchange significantly muddles both the model and analysis, as it must first be determined which water pool(s) the free water may exchange with (likely only the IE water pool). Beyond modeling complications, this will also introduce two additional free-parameters to the model, which significantly complicates fitting.

This paper has aimed to investigate the effect of including an additional free-parameter into the mcDESPOT framework, and to evaluate the ability to reliably and robustly solve the resultant nine parameter model using clinically acquired *in vivo* data. What remains unaddressed is the accuracy of this model. Unfortunately, addressing this issue is not straightforward. Phantoms, such as dairy cream, provide multiple relaxation species but have the additional confound of different resonant frequencies associated with each species. 'Wedge' phantoms containing different materials with different relaxation properties may also be used, but obtaining accurate information regarding exchange between the differing materials is difficult. One could consider more exotic phantoms, in which the relaxation parameters could be adjusted with gadolinium and exchange rates via temperature or pH. However, if one is predominantly concerned with estimates of myelin water fraction, at the expense of the other metrics, comparison with histology will provide the surest validation.

An important consideration in any quantitative imaging technique is its inter-scan repeatability and inter-subject variability, as both inform on sample sizes required for clinical studies as well as predictive power. In this work, the 3-pool results are shown to have high inter-scan reproducibility, with a average CoV of 5.9%. This is of particular importance to longitudinal studies of disease progression or treatment efficacy. Inter-subject variability was also shown to be low, with a mean CoV of 0.109. Further studies incorporating additional male and female participants will be required to definitely state the reproducibility of the approach. Of note, however, these results (and those of the numerical simulations) contradict a recent theoretical analysis of mcDESPOT precision (18). It is possible the difference in analysis approach (unconstrained in the theoretical analysis, vs. constrained here) is the reason behind the high precision observed here compared with predicted. We have evaluated the model over a range of pathological conditions and age-ranges and have not noticed a degradation in results.

Overall, we find that the 3-pool model agrees well with the conventional 2-pool approach in homogeneous tissue whilst improving the performance of the method in areas of partial volume. In light is this finding, we conclude that it is the preferred choice for future analysis.

Acknowledgments

This work was supported by the National Institutes of Mental Health (R01 MH087510) and the Medical Research Council, UK (G0800298). The authors thanks Drs. Carlo Pierpaoli and Alex MacKay for many important and insightful conversations.

Appendix A

The two-component models of the equilibrium SPGR and bSSFP magnetizations are given by Eqns. [1] and [2], respectively. For the SPGR model, only the longitudinal magnetization needs to be considered if ideal spoiling is assumed for the transverse magnetization. Under these conditions,

$$M_{SPGR}=\rho\begin{bmatrix} M_F & IE_F \end{bmatrix}^T \quad [A1]$$

and

$$A_{SPGR}=\begin{bmatrix} -\frac{1}{T_{1,M}}-k_{M\to IE} & k_{IE\to M} \\ k_{M\to IE} & -\frac{1}{T_{1,IE}}-k_{IE\to M} \end{bmatrix}. \quad [A2]$$

In the case of bSSFP, both the longitudinal *and* transverse magnetization components need to be considered, as both are driven to dynamic equilibrium. Under these conditions,

$$A_{bSSFP}=\begin{bmatrix} -\frac{1}{T_{2,M}}-k_{M\to IE} & k_{IE\to M} & \Delta\omega_M & 0 & 0 & 0 \\ k_{M\to IE} & -\frac{1}{T_{2,IE}}-k_{IE\to M} & 0 & \Delta\omega_{IE} & 0 & 0 \\ -\Delta\omega_M & 0 & -\frac{1}{T_{2,M}}-k_{M\to IE} & k_{M\to IE} & 0 & 0 \\ 0 & -\Delta\omega_{IE} & k_{M\to IE} & -\frac{1}{T_{2,IE}}-k_{IE\to M} & 0 & 0 \\ 0 & 0 & 0 & 0 & -\frac{1}{T_{1,M}}-k_{M\to IE} & k_{M\to IE} \\ 0 & 0 & 0 & 0 & k_{M\to IE} & -\frac{1}{T_{1,IE}}-k_{IE\to M} \end{bmatrix} \quad [A3]$$

and

$$C=\rho\begin{bmatrix} 0 & 0 & 0 & 0 & \frac{M_F}{T_{1,M}} & \frac{IE_F}{T_{1,IE}} \end{bmatrix}^T. \quad [A4]$$

In the above expressions, $k_{M\to IE}$ is the exchange rate from the myelin-associated to the intra/extra-cellular water pools; $k_{IE\to M}$ is the exchange rate from the intra/extra-cellular to the myelin-associated water pools; $\Delta\omega_M$ and $\Delta\omega_{IE}$ are the off-resonance values (with respect to the central water peak); and ρ is a term proportional to the equilibrium longitudinal magnetization. Assuming the close proximity of the water pools, we assume that $\Delta\omega = \Delta\omega_M = \Delta\omega_{IE}$.

Appendix B

To account for an addition third water component in the SPGR and bSSFP models, the M_{SPGR}, A_{SPGR}, A_{bSSFP}, and C matrices (Eqns. [A1] through [A4]) are expanded as

$$M_{SPGR}=\rho\begin{bmatrix} M_F & IE_F & 1-(M_F+IE_F) \end{bmatrix}^T, \quad \text{[B1]}$$

$$A_{SPGR}=\begin{bmatrix} -\frac{1}{T_{1,M}}-k_{M\to IE} & k_{IE\to M} & 0 \\ k_{M\to IE} & -\frac{1}{T_{1,IE}}-k_{IE\to M} & 0 \\ 0 & 0 & -\frac{1}{T_{1,F}} \end{bmatrix}, \quad \text{[B2]}$$

$$C=\rho\begin{bmatrix} 0 & 0 & 0 & 0 & 0 & 0 & \frac{M_F}{T_{1,M}} & \frac{IE_F}{T_{1,IE}} & \frac{F_F}{T_{1,F}} \end{bmatrix}^T, \quad \text{[B3]}$$

and

$$A_{bSSFP}=\begin{bmatrix} -\frac{1}{T_{2,M}}-k_{M\to IE} & k_{IE\to M} & 0 & \Delta\omega & 0 & 0 & 0 & 0 & 0 \\ k_{M\to IE} & -\frac{1}{T_{2,IE}}-k_{IE\to M} & 0 & 0 & \Delta\omega & 0 & 0 & 0 & 0 \\ 0 & 0 & -\frac{1}{T_{2,F}} & 0 & 0 & \Delta\omega & 0 & 0 & 0 \\ -\Delta\omega & 0 & 0 & -\frac{1}{T_{2,M}}-k_{M\to IE} & k_{IE\to M} & 0 & 0 & 0 & 0 \\ & -\Delta\omega & 0 & k_{M\to IE} & -\frac{1}{T_{2,IE}}-k_{IE\to M} & 0 & 0 & 0 & 0 \\ & & -\Delta\omega & 0 & 0 & -\frac{1}{T_{2,F}} & 0 & 0 & 0 \\ 0 & 0 & 0 & 0 & 0 & 0 & -\frac{1}{T_{1,M}}-k_{M\to IE} & k_{IE\to M} & 0 \\ 0 & 0 & 0 & 0 & 0 & 0 & k_{M\to IE} & -\frac{1}{T_{1,IE}}-k_{IE\to M} & 0 \\ 0 & 0 & 0 & 0 & 0 & 0 & 0 & 0 & -\frac{1}{T_{1,F}} \end{bmatrix} \quad \text{[B4]}$$

References

1. MacKay A, Laule C, Vavsour I, Bjarnason T, Kolling S, Madler B. Insights into Brain Microstructure from the T2 Distribution. Magn Reson Imag. 2006; 24:515–525.
2. Laule C, Leung E, Lis DK, Traboulsee AL, Paty DW, MacKay AL, Moore GR. Myelin Water Imaging in Multiple Sclerosis: Quantitative Correlations with Histopathology. Mult Scler. 2006; 12:747–753. [PubMed: 17263002]
3. Webb S, Munro CA, Midha R, Stanisz GJ. Is Multicomponent T2 a Good Measure of Myelin Content in Peripheral Nerve? Magn Reson Med. 2003; 49:638–645. [PubMed: 12652534]

4. Laule C, Vavasour IM, Leung E, Li DK, Kozlowski P, Traboulsee AL, Oger J, MacKay AL, Moore GR. Pathological Basis of Diffusely Abnormal White Matter: Insights from Magnetic Resonance Imaging and Histology. Mult Scler. 2011; 17:144–150. [PubMed: 20965961]
5. Kolind SH, Laule C, Vavasour IM, Li DK, Traboulsee AL, Madler B, Moore GR, MacKay AL. Complementary Information from Multi-Exponential T2 Relaxation and Diffusion Tensor Imaging Reveals Differences Between Multiple Sclerosis Lesions. NeuroImage. 2008; 40:77–85. [PubMed: 18226549]
6. Flynn SW, Lang DJ, macKay AL, Goghari V, Vavasour IM, Whittall KP, Smith GN, Arango V, Mann JJ, Dwork AJ, Falkai P, Honer WG. Abnormalities of Myelination in Schizophrenia Detected In Vivo with MRI, and Post-Mortem with Analysis of Aligodendrocyte Proteins. Mol Psychiatry. 2003; 8:811–820. [PubMed: 12931208]
7. Meyers SM, Laule C, Vavasour IM, Kolind SH, Madler B, Tam R, Traboulsee AL, Lee J, Li DK, MacKay AL. Reproducibility of Myelin Water Fraction Analysis: A Comparison of Region of Interest and Voxel-Based Analysis Methods. Magn Reson Imaging. 2009; 27:1096–1103. [PubMed: 19356875]
8. Deoni SCL, Rutt BK, Arun T, Pierpaoli C, Jones DK. Gleaning Multicomponent T1 and T2 Information from Steady-State Imaging Data. Magn Reson Med. 2008; 60:1372–1387. [PubMed: 19025904]
9. Deoni SCL. Correction of Main and Transmit Magnetic Field (B0 and B1) Inhomogeneity Effects in Multicomponent Driven Equilibrium Single Pulse Observation of T1 and T2. Magn Reson Med. 2011; 65:1021–1035. [PubMed: 21413066]
10. Lancaster JL, Andrews T, Hardies LJ, Dodd S, Fox PT. Three-Pool Model of White Matter. J Magn Reson Imag. 2003; 17:1–10.
11. Does MD, Gore JC. Compartmental Study of T1 and T2 in Rat Brain and Trigeminal Nerve In Vivo. Magn Reson Med. 2002; 47:274–283. [PubMed: 11810670]
12. Spencer RGS, Fishbein KW. Measurement of Spin-Lattice Relaxation Times and Concentrations in Systems with Chemical Exchange Using the One-Pulse Sequence: Breakdown of the Ernst Model for Partial Saturation in Nuclear Magnetic Resonance Spectrscopy. J Magn Reson. 2000; 142:120–135. [PubMed: 10617442]
13. Deoni SCL, Rutt BK, Jones DK. Investigating the Effect of Exchange and Multicomponent T1 Relaxation on the Short Repetition Time Spoiled Steady-State Signal and the DESPOT1 T1 Quantification Method. J Magn Reson Imaging. 2007; 25:570–578. [PubMed: 17326090]
14. Deoni SCL, Rutt BK, Jones DK. Investigating Exchange and Multicomponent Relaxation in Fully-Balanced Steady-State Free Precession Imaging. J Magn Reson Imaging. 2008; 27:1421–1429. [PubMed: 18504765]
15. Berger MF, Silverman HF. Microphone Array Optimization by Stochastic Region Contraction. IEEE Trans Signal Processing. 1991; 39:2377–2386.
16. McQuarrie, ADR.; Tsai, CL. Regression and Time Series Model Selection. Singapore: World Scientific; 1998.
17. Deoni SCL, Mercure E, Blasi A, Gasston D, Thomson A, Johnson M, Williams SC, Murphy DG. Mapping Infant Brain Myelination with Magnetic Resonance Imaging. J Neurosci. 2011; 31:784–791. [PubMed: 21228187]
18. Lankford CL, Does MD. On the Inherent Precision of mcDESPOT. Magn Reson Med. 2012 Ahead of Print.

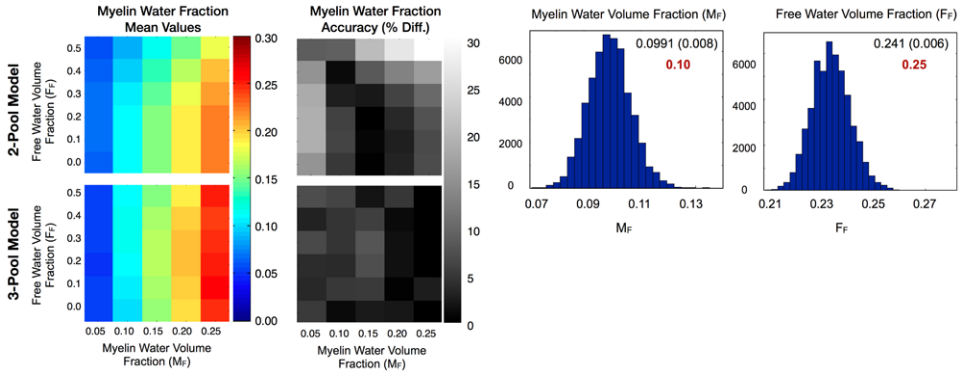

Figure 1.

Results from the numerical simulation comparing the 2 and 3-pool model myelin water fraction value accuracy over and range of myelin and free water fractions.

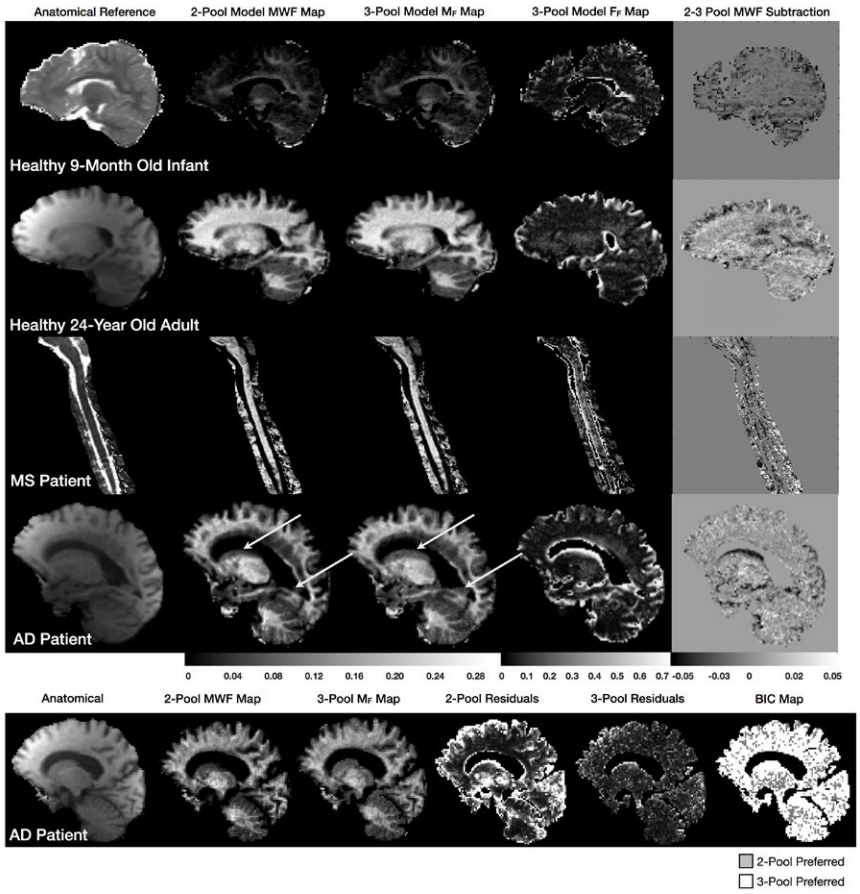

Figure 2.

Two and three-pool model derived myelin water fraction maps for the 9 month old infant, 24 year old adult, and MS and AD patients. Shown for each are corresponding reference anatomical, the calculated free water volume fraction map, and a myelin water fraction difference map calculated by subtracting the three-pool MWF map from the two-pool result.

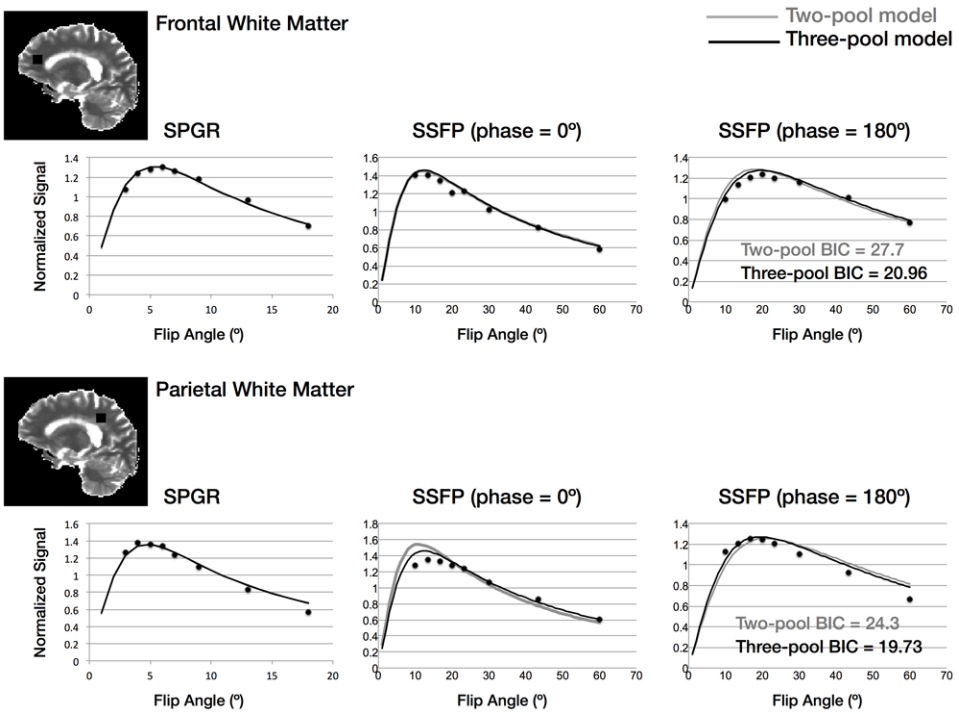

Figure 3.

Example raw data and reconstructed two and three-pool signal curves for two different brain regions. The two-pool model is shown by the grey line, the three-pool model by the dark line. The BIC metrics calculated for both cases show the three-pool model to be preferred.

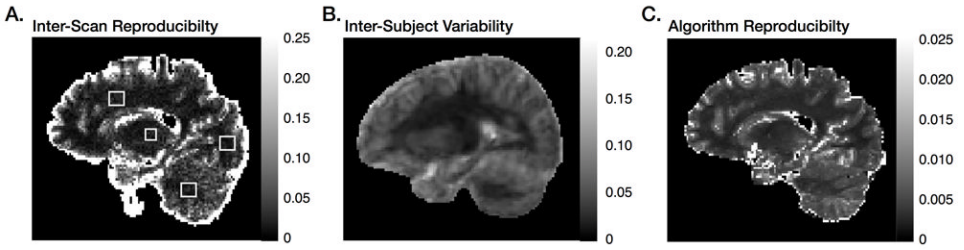

Figure 4.

Results from the (a) intra-scan; (b) inter-subject variability; and (c) algorithm reproducibility studies. Shown for each are maps of the coefficient of variation calculated from repeated measures. Outline boxes in (a) denote regions of interest used to determine the mean CoV (Table 1). For the inter-scan reproducibility, a mean CoV of 0.059 was calculated. Inter-subject variability was found to be 0.1 1; and for the algorithm reproducibility, a mean CoV of 0.09 was found.

Table 1

Mean inter-scan and inter-subject MWF coefficient of variation values obtained from the frontal, occipital and cerebellar white matter, and the thalamus. Regions are depicted in Fig. 4a.

Brain Region	**Inter-Scan CoV**	**Inter-Subject CoV**
Frontal White Matter	0.061	0.107
Occipital White Matter	0.051	0.093
Cerebellar White Matter	0.064	0.112
Thalamus	0.058	0.126
Average	*0.059*	*0.109*